

Combined multiplet and cumulant Green's function treatment of correlation effects in x-ray photoelectron spectroscopy

J. J. Kas,¹ J. J. Rehr,^{1,2} and T. P. Devereaux^{3,4}

¹*Dept. of Physics, Univ. of Washington Seattle, WA 98195-1560*

²*Department of Photon Science, SLAC National Accelerator Laboratory, Menlo Park, California 94025, USA*

³*Department of Materials Science and Engineering,
Stanford University, Stanford, California 94305, USA*

⁴*Stanford Institute for Materials and Energy Sciences,
SLAC National Accelerator Laboratory, Menlo Park, California 94025, USA*

(Dated: July 23, 2021)

The treatment of electronic correlations in open-shell systems is among the most challenging problems of condensed matter theory. Current approximations are only partly successful. Ligand field multiplet theory (LFMT) has been widely successful in describing intra-atomic correlation effects in x-ray spectra, but typically ignores itinerant states. The cumulant expansion for the one electron Green's function successfully describes shake-up effects but ignores atomic multiplets. More complete methods are computationally problematic. Here we show that separating the dynamic Coulomb interactions into local and longer-range parts yields an efficient, nearly *ab initio* multiplet + cumulant approach that accounts for both local atomic multiplet-splittings and charge-transfer shake-up satellites. An application to α -Fe₂O₃ (hematite) yields very good agreement with XPS experiment, including the broad 9 eV satellites and distributed background features missing from previous approaches.

PACS numbers: 71.15.-m, 31.10.+z, 71.10.-w

Keywords: Green's function, cumulant, GW, DFT, excited states

The frontier of an *in-silico* description of complex functional behavior of materials lies in a consistent description of their physics and chemistry over many length and time scales. Achieving such a description has been a major challenge of computational materials science, whose success is ultimately assessed by the ability to describe both ground and excited states, including non-equilibrium conditions¹. Computational methods typically focus on delocalized band-like descriptions, as in Kohn-Sham density functional theory (DFT), or highly localized descriptions, as in ligand-field multiplet theory (LFMT)² and quantum chemistry^{3,4}. However, more elaborate approaches such as dynamical mean field theory (DMFT)^{5,6} and embedding methods extended to clusters^{7,8} have been used to move away from purely local or delocalized points of view. Both aspects are important in x-ray spectroscopy, which can provide atom-specific information about local coordination, valency, and excited states that is well captured by multiplet approaches for deep core states^{2,9}. Computational schemes that combine these aspects are highly desirable for strongly correlated materials such as transition metal oxides (TMOs). This is the main goal of this work, where a local LFMT model is combined with the non-linear cumulant Green's function approach¹⁰⁻¹³ to treat both local- and longer-range correlated behavior.

Core-level x-ray photoemission spectroscopy (XPS) is a sensitive probe of correlation effects in excited state electronic structure. In particular, the XPS signal is directly related to the core-level spectral function $A_c(\omega)$, which describes the distribution of excitations in a material. The main peak in the XPS corresponds to the

quasiparticle, while secondary features, i.e., satellites, correspond to many-body excitations. These satellite features are pure many-body correlation effects which have proved difficult to calculate from first principles in strongly correlated materials. They can also have considerable spectral weight, comparable to that in the main peak and spread over a broad range of energies. Many-body perturbation theory within the GW approximation is inadequate to treat these effects. While GW can give reasonably accurate core-level binding energies (quasiparticle energies)^{14,15}, the satellite positions and amplitudes are not well reproduced, even in relatively weakly correlated systems such as sodium and silicon. On the other hand, the cumulant expansion of the one-electron Green's function¹⁶⁻¹⁸ has shown notable success in predicting the quasi-bosonic satellite progressions seen in those systems^{10,19-23}, as well as the charge-transfer satellites observed in some TMOs^{24,25}. Nevertheless an accurate treatment of the excitation spectrum of strongly correlated materials typically demands more elaborate theories, such as CI³, coupled-cluster techniques^{26,27}, or by mapping electronic structure from DFT or GW calculations onto model Hamiltonians, as in *ab initio* LFMT²⁸⁻³¹. These approaches can yield impressive results for multiplet splittings from localized states as seen in XPS; however, they generally lack an adequate Hilbert space to fully account for extended states and collective excitations. While dynamical processes such as charge-transfer excitations can be treated with model Hamiltonians as in cluster LFMT, or LDA+DMFT^{7,32}, the inclusion of high energy excitations is numerically challenging⁶.

In an effort to address these limitations, we introduce here an approach that combines a simplified local multiplet model that ignores charge transfer effects, with the cumulant approximation for the core-Green's function. We dub the approach *Multiplet+C*, in analogy with other methods where the cumulant Green's function is added to treat satellite excitations^{10,19,21,33}. As a consequence, this combined method treats both local electronic correlations and dynamical excitations of the extended system. The approach is also advantageous computationally and simplifies the physical interpretation. For simplicity, we focus our attention on the $2p$ XPS of TMOs, where the number of $2p$ electrons changes from 6 to 5 upon photo-excitation. Using a separation of the short- and long-ranged Coulomb interactions, the method yields an expression for the core spectral function $A_{2p}(\omega) = -(1/\pi)\text{Im}G_{2p}(\omega)$ given by a convolution of the $2p$ local spectral function with the cumulant spectral function for the extended system,

$$A_{2p}(\omega) = A_{2p}^{\text{loc}}(\omega) * A_{2p}^C(\omega). \quad (1)$$

As a consequence, each discrete local level is broadened by the cumulant spectral function $A_{2p}^C(\omega)$, which also produces shake satellites. Our calculations are carried out in the time-domain¹², where the Green's function is given by the cumulant ansatz,

$$G_{2p}(t) = G_{2p}^{\text{loc}}(t)e^{C_{2p}(t)}, \quad (2)$$

where $G_{2p}^{\text{loc}}(t)$ is the trace over $2p$ single particle states of the atomic multiplet Green's function for our simplified model, and $C_{2p}(t)$ is the cumulant, which builds in dynamic correlation effects. The above approximation was inspired by the work in Refs.^{6,34}, where a similar product of an atomic Green's function and cumulant form was used to treat plasmon excitations in DMFT. To justify our approach we define a separable model Hamiltonian $H = H^{\text{loc}} + H^{\text{bos}}$ in which the simplified localized (atomic, ligand field, or cluster) system consists of a limited number of electrons (the $2p$ and $3d$ shells for example) interacting with the extended system via quasi-bosons that characterize the excitations¹⁰. In the results presented here, the local system is defined by a short-range many-body Hamiltonian,

$$H^{\text{loc}} = \sum_i \epsilon_i n_i + \sum_{i,j} [V_{i,j}^{\text{xf}} c_i^\dagger c_j + c.c.] + \sum_{i,j,k,l} v_{ijkl} c_i^\dagger c_j^\dagger c_k c_l, \quad (3)$$

where V^{xf} denotes the crystal field potential, v the Coulomb interaction, and the electron levels $\{i, j\}$ are limited to the $2p$ and $3d$ shells of a single atom. In general, this Hamiltonian can be extended to include ligands as in *ab initio* LFMT or cluster CI calculations. However, we find that for the results presented here (XPS of Fe_2O_3), it is sufficient to simply scale the Slater-Condon parameters to match the *ab initio* cluster CI results of Bagus et al.³⁵ (see supplementary information for comparison), which did not include shake satellites. Thus

H^{loc} accounts for covalency effects on the multiplet levels, but does not treat charge transfer satellites which are included via the cumulant. This approximation allows a simple solution of the problem, although it does not include the effects of charge transfer on the local configuration, and instead keeps a fixed number of d -electrons within the local Hamiltonian. The quasi-boson Hamiltonian for the extended system including the coupling to the localized system is defined as

$$H^{\text{bos}} = \sum_q \omega_q a_q^\dagger a_q + \sum_{qi} n_i V_i^q (a_q^\dagger + a_q), \quad (4)$$

where V_i^q are fluctuation potentials¹⁰, and n_i is the occupation of the hole-state $i \in 2p$. If we now make the approximation that the couplings V_i^q are independent of the hole state i of the localized system, the net coupling depends only on the total number of holes $N_h = \sum_i n_i$ in the $2p$ shell, which is equal to 1 in the XPS final state. Then the Hamiltonian H^{bos} is equivalent to that of Langreth¹⁷, which describes a system of bosons interacting with an isolated core-electron. Notably, this model can be solved using a cumulant Green's function, with a cumulant proportional to the density-density correlation function $\chi(q, q', \omega)$. This yields a spectral function with a series of satellites corresponding to bosonic excitations. The difference in our treatment is that the localized system has its own set of eigenstates (the atomic-multiplet levels) once the $2p$ hole appears, each with its own bosonic satellites from the convolution with $A_{2p}^C(\omega)$. In our calculations the cumulant $C_{2p}(t)$ is obtained using real-time TDDFT approach analogous to the Langreth formulation²⁴, and can be expressed in Landau form³⁶,

$$C_{2p}(t) = \int d\omega \frac{\beta(\omega)}{\omega^2} [e^{-i\omega t} + i\omega t - 1], \quad (5)$$

$$\beta(\omega) = \omega \int d^3r \text{Re}[V(r)\delta\rho(\mathbf{r}, \omega)].$$

Here $\delta\rho(\mathbf{r}, \omega)$ is the time-Fourier transform of the density fluctuations $\delta\rho(r, t)$ induced by the sudden appearance of the core-hole, and $V(r)$ is the $2p$ core-hole potential. In order to treat the strong core-hole effects in correlated systems, we also include non-linear corrections to the cumulant, following the approach of Tzavala et al.¹³.

As an illustrative example, we apply this approach to the $2p$ XPS of $\alpha\text{-Fe}_2\text{O}_3$ (hematite). The localized system is treated with an atomic multiplet approach using modified Slater-Condon parameters F and G scaled by 0.8 to simulate the effects of covalency³⁷ and ignoring charge-transfer coupling. These parameters are calculated using a modified version of Desclaux's Dirac-Fock atomic code^{11,38,39}, available within the FEFF10 software package^{40,41}. We used a crystal field strength $10Dq = 0.5$ eV⁴², and spin-orbit couplings from the literature⁴³. The multiplet spectra obtained with this effective atomic model is found to be in quantitative agreement with the cluster CI calculations of Bagus et al.³⁵ that also ignore the charge-transfer coupling. Further details are reported in the Supplemental Material at

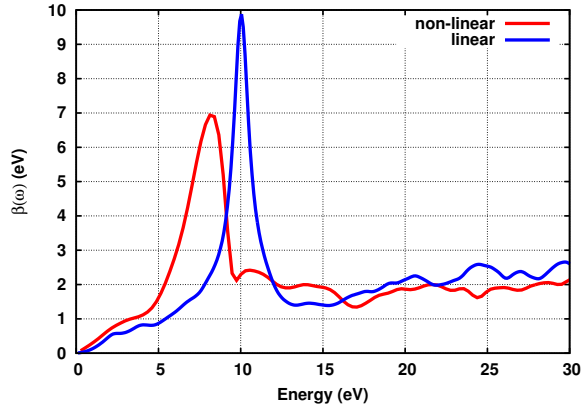


FIG. 1: Quasi-boson excitation spectrum $\beta(\omega)$ of Eq. (5) calculated within linear- (blue) and non-linear (red) response using the RT-TDDFT approach¹².

[URL will be inserted by publisher]. Within our simplified model Hilbert space, there are no excitations due to charge transfer from the localized system to the surroundings or vice versa. Consequently the spherical contributions to the direct interactions F_{pd}^0 and F_{dd}^0 only contribute to overall static shifts in the spectrum but not satellite structure. Thus in order to avoid double counting in the calculation of shake-up or charge-transfer satellites, we only use the spherical part of the Coulomb interaction when calculating the density response $\delta\rho(t)$ to the suddenly created core-hole at $t = 0$.

Our calculations of $\beta(\omega)$ are shown in Fig. 1. Note that the non-linear corrections further broaden and red-shift

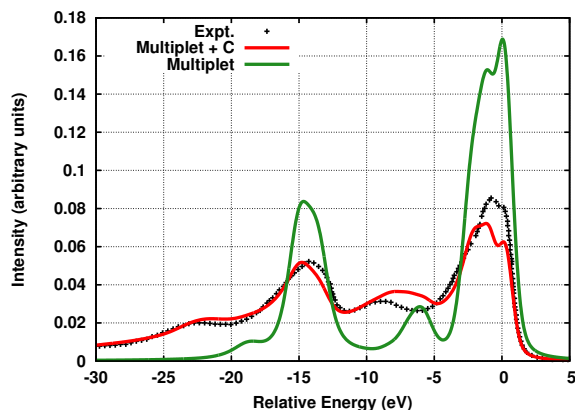


FIG. 2: Comparison of the area normalized $2p$ XPS of $\alpha\text{-Fe}_2\text{O}_3$ ³⁵ from experiment (black crosses) with that calculated using the CI-LFMT³⁵ (green) and the *Multiplet+C* approaches (red).

the main satellite in the direction of the -9 eV peak in the experimental XPS. Thus $\beta(\omega)$ differs from that based on linear response and the GW approximation where $\beta^{GW}(\omega) = (1/\pi)|\text{Im}\Sigma^{GW}(\omega + \epsilon_c)|$ ¹⁰. In Figure 2 we compare the experimental XPS spectrum of $\alpha\text{-Fe}_2\text{O}_3$ (digitally reproduced from Ref.⁴⁴) with that calculated using our *Multiplet+C* approach and with our local atomic multiplet model. The most noticeable differences are the broad satellites at roughly 9 eV below each of the main ($2p_{1/2}$ and $2p_{3/2}$) peaks. Moreover, consistent with the behavior of $\beta(\omega)$ in Fig. 1, there is a long-tail extending well beyond the -9 eV satellite that contributes to the intensity underneath the main peaks. These properties reflect the different time-scales and dynamic correlation effects involved in the local and shake-up processes. Upon convolution with the multiplet spectral function, these satellites yield replicas of the local spectra at 9 eV lower energy. In contrast the CI-LFMT spectra that ignore charge-transfer³⁵ has a weak multiplet feature at about -6 eV and no background.

The Landau representation in Eq. (5) facilitates the interpretation of the cumulant spectral function. From the structure of $C_{2p}(t)$, the kernel $\beta(\omega)$ corresponds to the transfer of oscillator strength from the quasi-particle peak to the satellites at frequency ω . The renormalization constant $Z = \exp(-a)$ describes the intensity of the quasi-particle peak, where $a = \exp[\int d\omega \beta(\omega)/\omega^2]$ is the dimensionless satellite strength, while $\Delta = \int d\omega \beta(\omega)/\omega$ is a correlation energy shift. Calculations of these values indicate substantial many-body effects, with of $a = 1.60$, $Z = 0.20$, $\Delta = 9.0$ eV, and an overall shake weight $1 - Z = 0.80$. However, as seen in Fig. 1, $\beta(\omega)$ also contains a nearly linear term at low energies from particle-hole excitations; this gives rise to an asymmetric, Doniach-Sunjic like main peak and a long tail, as in edge-singularity behavior. To differentiate this effect from the shake-up satellites, we redefine the quasiparticle peak to include the asymmetric line-shape by separating $\beta(\omega)$ into a low energy structure-less quasiparticle term $\beta_{qp}(\omega)$ and a higher energy satellite term $\beta_{sat}(\omega)$, following the treatment of Kas et al.²⁵. Further details are given in the Supplemental Material at [URL will be inserted by publisher]. The total cumulant spectral function is then given by an additional convolution of the asymmetric quasiparticle spectral function $A_{qp}(\omega)$ and a satellite spectral function $A_{sat}(\omega)$, as shown in Fig. 3. Once this separation is carried out, we find a quasiparticle renormalization constant $Z = 0.57$, $a = 0.57$, and a shake weight 0.43, in good agreement with the estimate of Bagus et al. $a = 0.4$ ³⁵. Note that there is also a second satellite at ~ 16 eV in both the full and satellite spectral functions. This reflects the excitation of two quasi-bosons (i.e., here a double charge transfer excitation). This second satellite is also seen in the $1s$ XPS of hematite (Fig. 3)⁷, although it is more pronounced in the experiment. To characterize its nature, it is useful to analyze the induced charge associated with the main shake satellite at -9 eV following creation of the $2p$ core hole. To this end,

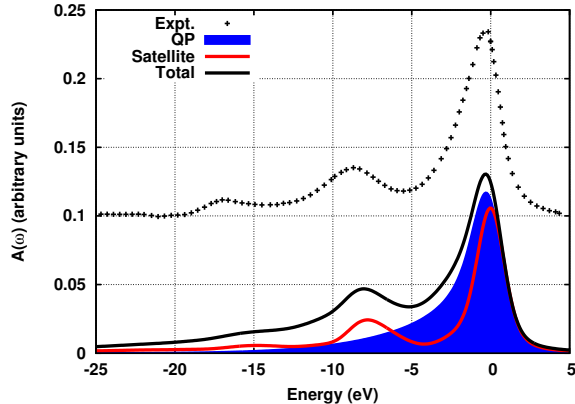


FIG. 3: Separation of the cumulant spectral function $A^C(\omega)$ (black) into quasiparticle, $A_{qp}(\omega)$ (red filled) and satellite, $A_{sat}(\omega)$ (blue) spectral functions. The full cumulant spectral function is then a convolution of A_{qp} and A_{sat} . In the figure, A_{qp} and A_{sat} have been scaled by the quasiparticle renormalization Z , and $1 - Z$ respectively, to facilitate comparison with the full cumulant spectral function. Note that the spectral function is in good agreement with the $1s$ XPS of Fe_2O_3 .

we calculate the fluctuations in the Mulliken charges (Fig. 4) vs time on the central Fe atom (red), the 6 O-ligand atoms (blue), as well as the sum of Fe and O-ligands (green). Within a fraction of a femtosecond, the electron count on the Fe increases by 1., then oscillates between 1. and 1.5 at a frequency $\omega_{CT} \sim 9$ eV, corresponding to charge-transfer fluctuations. In contrast, the oscillations in the O-ligand count are 180° out of phase, indicating a substantial charge transfer between metal and ligand. Note, however, that the sum of ligand and metal counts (green) contains sizable residual oscillations, indicating additional charge transfer from outer shells. In addition, the sum retains most of the initial increase seen in the Fe atom, suggesting that the transient screening in the first fraction of a femtosecond is collective in nature. Finally, although not shown, the oscillations are dominated by the minority spin channel on the Fe atom. This is not surprising, as the majority spin channel has only a small number of unoccupied d -states.

In conclusion, we have developed a combined *Multiplet+C* approach that treats the complementary short- and longer-ranged excited state correlation effects in open-shell systems. The method is based on the separation of the many-body Hamiltonian into that for a local many-body atomic system coupled to an extended system in terms of quasi-bosonic excitations as in the Langreth cumulant, that characterize the density fluctuations of the extended system. The approach yields a spectral function for the full system as a convolution of the local multiplet spectral function and the non-linear cumulant spectral function for the extended system. Thus

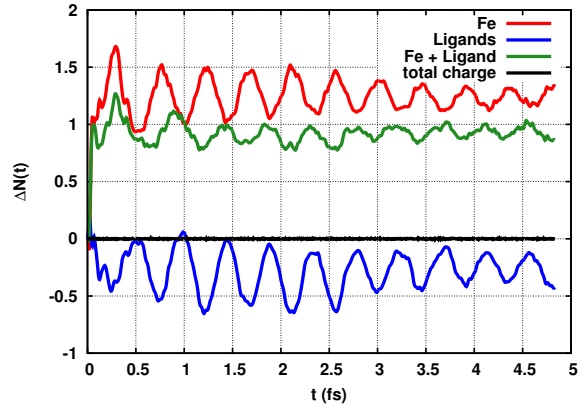


FIG. 4: Fluctuation in Mulliken counts $\Delta N(t)$ on the central Fe atom (red), the 6 O-ligands (blue), sum of Fe and O-ligands (green), and total (black) (which is zero to high accuracy). Note that these counts with period ~ 0.46 fs oscillate at the charge-transfer frequency $\omega_{CT} \sim 9$ eV.

each multiplet level of the local system is treated as a quasi-particle with its own spectral function and series of quasi-bosonic satellites. In this sense, the *Multiplet+C* approach is *doubly dynamic*, as in the DMFT+cumulant approach⁶. An application to hematite, a prototypical correlated TMO, yields $1s$ and $2p$ XPS spectra in very good agreement with experiment. In contrast to CI-based LFMT³⁵, Cluster-LFMT, or LDA+DMFT⁷, our approach simplifies the calculations and physical interpretation of the spectra, yet accounts quantitatively for the large shake excitations, double-excitations, and the broad background, with a weight comparable to that in the quasi-particle peak. Many extensions are possible; for example, the local model used here can be improved to treat clusters of atoms; the convolution with the cumulant spectral function can be applied *ex post facto* to treat collective excitations in other theoretical approaches; and the method can be applied to other x-ray spectra. Finally, we note that the results presented here provide proof of principle for an efficient *ab initio* approach to charge-transfer LFMT, since the only free parameters in the calculation (other than broadening) were used to match cluster calculations that did not include any shake or charge-transfer excitations.

Acknowledgments: We thank P. Bagus, F.M.F. de Groot, M. Haverkort, A. Hariki, and J. Lischner, L. Reining, and E. Shirley, for helpful comments. This work was developed with support from the Theory Institute for Materials and Energy Spectroscopies (TIMES) at SLAC, funded by the U.S. DOE, Office of Basic Energy Sciences, Division of Materials Sciences and Engineering under contract EAC02-76SF0051.

Appendix: Derivation of the Multiplet + C Green's function

The $2p$ XPS is given by the partial trace over the states of the $2p$ shell of the Green's function, i.e., $I_{2p}^{\text{XPS}}(\omega) \propto -\frac{1}{\pi} \text{Im}G_{2p}(\omega) = -\frac{1}{\pi} \sum_{i \in 2p} \text{Im}G_{ii}(\omega)$, where $G_{ii}(\omega)$ is the Fourier transform of the real-time Green's function,

$$G_{ii}(t) = -ie^{-iE_0 t} \langle 0 | c_i^\dagger e^{iHt} c_i | 0 \rangle. \quad (\text{A.1})$$

Here $|0\rangle$ is the ground state with associated energy E_0 , and the Hamiltonian we take as,

$$H = H^{\text{loc}} + H^{\text{bos}}, \quad (\text{A.2})$$

where H^{loc} describes a limited set of localized electronic states, and H_{bos} describes bosonic or quasi-bosonic excitations, i.e., plasmons, charge-transfer excitations, phonons, etc.,

$$H^{\text{loc}} = \sum_i \epsilon_i n_i + \sum_{i,j} [V_{i,j}^{\text{xf}} c_i^\dagger c_j + c.c.] + \sum_{i,j,k,l} v_{ijkl} c_i^\dagger c_j^\dagger c_k c_l, \\ H_{\text{bos}} = \sum_q \omega_q a_q^\dagger a_q + \sum_{q,i \in 2p} n_i V_i^q (a_q^\dagger + a_q). \quad (\text{A.3})$$

In the above, V_i^q are the fluctuation potentials, which couple the $2p$ hole i to the bosons q , c_i^\dagger/c_i are electron creation/annihilation operators, and a_q^\dagger/a_q are boson creation/annihilation operators. If we assume that $V_i^q = V^q$ is independent of the hole state, the boson Hamiltonian becomes,

$$H_{\text{bos}} = \sum_q \omega_q a_q^\dagger a_q + \sum_q N_h V^q (a_q^\dagger + a_q), \quad (\text{A.4})$$

where N_h is the total number of $2p$ holes, equal to 0 in the ground state, and 1 in the XPS final state. Now the entire problem simplifies since H^{loc} and H^{bos} commute in the XPS final state, and the Green's function is given by,

$$G_{2p}(t) = -ie^{-iE_0 t} \sum_{i \in 2p} \langle 0 | c_i^\dagger e^{iH^{\text{loc}} t} e^{iH^{\text{bos}} t} c_i | 0 \rangle. \quad (\text{A.5})$$

In addition, the ground state is the zero hole, zero boson state, and can be written $|\Psi_0\rangle|\nu_0\rangle$. Thus the Green's function becomes separable,

$$G_{2p}(t) = iG_{2p}^{\text{loc}}(t)G^{\text{bos}}(t), \\ G_{2p}^{\text{loc}}(t) = -ie^{-iE_0 t} \sum_{i \in 2p} \langle \Psi_0 | c_i^\dagger e^{iH^{\text{loc}} t} c_i | \Psi_0 \rangle, \\ G^{\text{bos}}(t) = -i \langle \nu_0 | e^{iH^{\text{bos}} t} | \nu_0 \rangle = -ie^{C(t)}. \quad (\text{A.6})$$

The local Green's function can be calculated via exact diagonalization or iterative inversion schemes such as Lanczos. The Green's function of the bosons is identical to that of Langreth for an isolated core-electron interacting with bosons, and can be found analytically¹⁷. Finally, taking the Fourier transform, the XPS intensity can be written,

$$I_{2p}^{\text{XPS}}(\omega) \propto A_{2p}(\omega) = A^{\text{loc}}(\omega) * A^{\text{bos}}(\omega). \quad (\text{A.7})$$

Appendix: Multiplet Calculations

Ligand-field multiplet theory (LFMT) calculations were carried out with the WebXRS code^{45,46}. The Slater-Condon parameters were calculated based on a Fe^{3+} atom with using the Dirac-Fock atomic code available within the FEFF10 package. In order to take covalency into account, the Slater-Condon parameters were reduced to 85% of the value as calculated for the Fe^{3+} ion, which produces a spectrum that closely matches that for an FeO_6 cluster calculated by Bagus et al.³⁵, as shown in Fig. 5. The values of all parameters necessary to define the local atomic multiplet Hamiltonian are shown in table I.

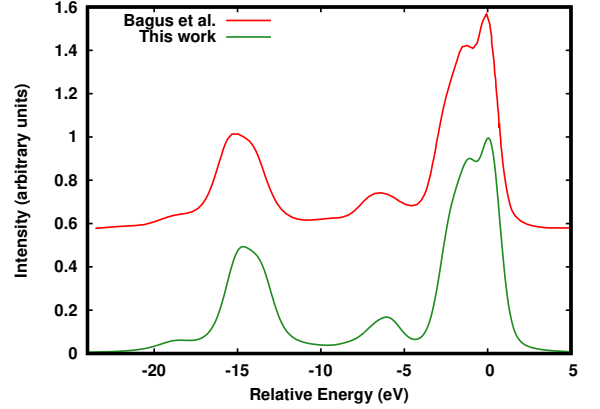


FIG. 5: Comparison of the LFMT spectral functions calculated using the CI-LFMT calculations of Bagus et al. (red)³⁵ and the atomic LFMT calculations using the Slater-Condon parameters of this work (green).

$10Dq$	0.5
ζ_{2p}	8.2
ζ_{3d}	0.06
F_{dd}^2	10.4
F_{dd}^4	6.5
F_{pd}^2	5.9
G_{pd}^1	4.32431
G_{pd}^3	2.4

TABLE I: Parameters used in LFMT calculations for Fe^{3+} from this work.

Appendix: Real-Time TDDFT calculations

The real-time TDDFT calculations were performed with the real-time version of the SIESTA code^{24,47}. using the PBE generalized gradient functional⁴⁸. The default

double-zeta plus polarization (DZP) basis set was used for both Fe and O atoms. In order to limit the interaction of the core-holes, a 3x3x3 supercell consisting of 270 atoms was used, which was found to produce converged spectra. The pseudopotentials were calculated using the ATOM code⁴⁹ with parameters taken from Rivero et al.⁵⁰.

Appendix: Separation of the cumulant spectral function

In order to separate the cumulant spectral function into quasiparticle and satellite parts we assume a simple separation of the quasi-boson excitation spectrum, i.e.,

$$\begin{aligned}\beta(\omega) &= \beta_{\text{sat}}(\omega) + \beta_{\text{QP}}(\omega), \\ \beta_{\text{QP}}(\omega) &= \alpha\omega e^{-\omega^2/\omega_0^2},\end{aligned}\quad (\text{A.1})$$

where α is set to match the linear portion of $\beta(\omega)$ near the origin, and ω_0 was set to the energy of the charge-transfer

peak at 8.5 eV. The quasiparticle portion β_{QP} contains all of the low frequency weight which produces the asymmetry in the main peak of the spectral function, while the satellite portion, β_{sat} contains the majority of the weight related to the main quasi-bosonic (charge-transfer) excitation. Note that this separation is not unique, but does not effect the total spectrum, and only effects the definition of shake up weight in the satellite, and the quasiparticle properties such as the renormalization.

Appendix: Broadening of the spectra

All spectra were broadened with Voigt functions using a Gaussian full-width full-max (FWFM) of 1.2 eV to account for experimental broadening and coupling to phonons. The Lorentzian broadening was set to 0.41 eV FWFM for the $2p_{3/2}$ portion of the spectrum, above ≈ -10 eV, and increased to 1.14 eV below that to account for the larger lifetime width of the $2p_{1/2}$ states.

-
- ¹ R. M. Martin, L. Reining, and D. M. Ceperley, *Interacting Electrons: Theory and Computational Approaches* (Cambridge University Press, Cambridge, 2016).
- ² F. de Groot and A. Kotani, *Core Level Spectroscopy of Solids* (CRC Press, 2008).
- ³ P. S. Bagus, E. S. Ilton, and C. J. Nelin, *Surface Science Reports* **68**, 273 (2013), ISSN 0167-5729.
- ⁴ J. F. Stanton and R. J. Bartlett, *J. Comp. Phys.* **98**, 7029 (1993), <https://doi.org/10.1063/1.464746>.
- ⁵ A. Georges, G. Kotliar, W. Krauth, and M. J. Rozenberg, *Reviews of Modern Physics* **68**, 13 (1996).
- ⁶ M. Casula, A. Rubtsov, and S. Biermann, *Phys. Rev. B* **85**, 035115 (2012).
- ⁷ M. Ghiasi, A. Hariki, M. Winder, J. Kuneš, A. Regoutz, T.-L. Lee, Y. Hu, J.-P. Rueff, and F. M. F. de Groot, *Phys. Rev. B* **100**, 075146 (2019).
- ⁸ A. Hariki, T. Uozumi, and J. Kuneš, *Phys. Rev. B* **96**, 045111 (2017).
- ⁹ E. L. Shirley, *Journal of electron spectroscopy and related phenomena* **144**, 1187 (2005).
- ¹⁰ L. Hedin, *J. Phys.: Condens. Matter* **11**, R489 (1999).
- ¹¹ Z. Zhou, J. Kas, J. Rehr, and W. Ermler, *Atomic Data and Nuclear Data Tables* **114**, 262 (2017).
- ¹² J. J. Kas, J. J. Rehr, and L. Reining, *Phys. Rev. B* **90**, 085112 (2014).
- ¹³ M. Tzavala, J. J. Kas, L. Reining, and J. J. Rehr, *Phys. Rev. Research* **2**, 033147 (2020).
- ¹⁴ M. J. van Setten, R. Costa, F. Viñes, and F. Illas, *Journal of Chemical Theory and Computation* **14**, 877 (2018), pMID: 29320628, <https://doi.org/10.1021/acs.jctc.7b01192>.
- ¹⁵ D. Golze, L. Keller, and P. Rinke, *The Journal of Physical Chemistry Letters* **11**, 1840 (2020), pMID: 32043890, <https://doi.org/10.1021/acs.jpcl.9b03423>.
- ¹⁶ P. Nozières and C. T. de Dominicis, *Phys. Rev.* **178**, 1097 (1969).
- ¹⁷ D. C. Langreth, *Phys. Rev.* **182**, 973 (1969).
- ¹⁸ C.-O. Almbladh and L. Hedin, *Handbook on Synchrotron Radiation* **1**, 686 (1983).
- ¹⁹ M. Guzzo, G. Lani, F. Sottile, P. Romaniello, M. Gatti, J. J. Kas, J. J. Rehr, M. G. Silly, F. Sirotti, and L. Reining, *Phys. Rev. Lett.* **107**, 166401 (2011).
- ²⁰ M. Guzzo, J. J. Kas, L. Sponza, C. Giorgetti, F. Sottile, D. Pierucci, M. G. Silly, F. Sirotti, J. J. Rehr, and L. Reining, *Phys. Rev. B* **89**, 085425 (2014).
- ²¹ J. Lischner, D. Vigil-Fowler, and S. G. Louie, *Phys. Rev. B* **89**, 125430 (2014).
- ²² J. S. Zhou, L. Reining, A. Nicolaou, A. Bendounan, K. Ruotsalainen, M. Vanzini, J. J. Kas, J. J. Rehr, M. Muntwiler, V. N. Strocov, et al., *Proceedings of the National Academy of Sciences* **117**, 28596 (2020), ISSN 0027-8424, <https://www.pnas.org/content/117/46/28596.full.pdf>.
- ²³ F. Caruso, C. Verdi, and F. Giustino (Springer International Publishing, Cham, 2020), pp. 341–365, ISBN 978-3-319-44677-6.
- ²⁴ J. J. Kas, F. D. Vila, J. J. Rehr, and S. A. Chambers, *Phys. Rev. B* **91**, 121112(R) (2015).
- ²⁵ J. J. Kas, J. J. Rehr, and J. B. Curtis, *Phys. Rev. B* **94**, 035156 (2016).
- ²⁶ J. J. Rehr, F. D. Vila, J. J. Kas, N. Y. Hirshberg, K. Kowalski, and B. Peng, *The Journal of Chemical Physics* **152**, 174113 (2020).
- ²⁷ F. D. Vila, J. J. Rehr, J. J. Kas, K. Kowalski, and B. Peng, *Journal of Chemical Theory and Computation* **16**, 6983 (2020).
- ²⁸ M. W. Haverkort, M. Zwierzycki, and O. K. Andersen, *Phys. Rev. B* **85**, 165113 (2012).
- ²⁹ H. Ikeno, T. Mizoguchi, and I. Tanaka, *Phys. Rev. B* **83**, 155107 (2011).
- ³⁰ S. K. Singh, J. Eng, M. Atanasov, and F. Neese, *Coordination Chemistry Reviews* **344**, 2 (2017).

- ³¹ P. Krüger, *Radiation Physics and Chemistry* **175**, 108051 (2020).
- ³² O. Šipr, J. Minár, A. Scherz, H. Wende, and H. Ebert, *Phys. Rev. B* **84**, 115102 (2011).
- ³³ F. Aryasetiawan, L. Hedin, and K. Karlsson, *Phys. Rev. Lett.* **77**, 2268 (1996).
- ³⁴ S. Biermann and A. van Rooykeghem, *Journal of Electron Spectroscopy and Related Phenomena* **208**, 17 (2016).
- ³⁵ P. S. Bagus, C. J. Nelin, C. R. Brundle, N. Lahiri, E. S. Ilton, and K. M. Rosso, *The Journal of Chemical Physics* **152**, 014704 (2020).
- ³⁶ L. Landau, *J. Phys. USSR* **8**, 201 (1944).
- ³⁷ S. Wang, W. L. Mao, A. P. Sorini, C.-C. Chen, T. P. Devereaux, Y. Ding, Y. Xiao, P. Chow, N. Hiraoka, H. Ishii, et al., *Phys. Rev. B* **82**, 144428 (2010).
- ³⁸ A. Ankudinov, S. Zabinsky, and J. Rehr, *Computer physics communications* **98**, 359 (1996).
- ³⁹ J. Desclaux, *Atomic data and nuclear data tables* **12**, 311 (1973).
- ⁴⁰ J. J. Kas, F. D. Vila, C. D. Pemmaraju, T. S. Tan, and J. J. Rehr, Submitted **XX**, xxxx (2021).
- ⁴¹ J. J. Kas, F. D. Vila, C. D. Pemmaraju, T. S. Tan, and J. J. Rehr, arXiv:cond-mat p. 2106.1334 (2021).
- ⁴² A. S. M. Ismail, Y. Uemura, S. H. Park, S. Kwon, M. Kim, H. Elnaggar, F. Frati, Y. Niwa, H. Wadati, Y. Hirata, et al., *Phys. Chem. Chem. Phys.* **22**, 2685 (2020).
- ⁴³ M. Haverkort, Ph.D. thesis, Universität zu Köln (2005).
- ⁴⁴ P. S. Bagus, C. J. Nelin, C. R. Brundle, N. Lahiri, E. S. Ilton, and K. M. Rosso, *The Journal of Chemical Physics* **152**, 014704 (2020).
- ⁴⁵ S. Wang, W. L. Mao, A. P. Sorini, C.-C. Chen, T. P. Devereaux, Y. Ding, Y. Xiao, P. Chow, N. Hiraoka, H. Ishii, et al., *Phys. Rev. B* **82**, 144428 (2010), URL <https://link.aps.org/doi/10.1103/PhysRevB.82.144428>.
- ⁴⁶ T. P. Devereaux, B. Moritz, C. Jia, J. J. Kas, and J. J. Rehr, submitted **xx**, xxxxx (2021).
- ⁴⁷ Y. Takimoto, F. D. Vila, and J. J. Rehr, *J. Chem. Phys.* **127**, 154114 (2007).
- ⁴⁸ J. P. Perdew, K. Burke, and M. Ernzerhof, *Phys. Rev. Lett.* **77**, 3865 (1996).
- ⁴⁹ *The ATOM pseudopotential code*, URL https://siesta-project.org/SIESTA_MATERIAL/Pseudos/atom_licence.html.
- ⁵⁰ P. Rivero, V. M. García-Suárez, D. Pereñiguez, K. Utt, Y. Yang, L. Bellaiche, K. Park, J. Ferrer, and S. Barraza-Lopez, *Computational Materials Science* **98**, 372 (2015), ISSN 0927-0256.